Final revised version for publication, submitted to JGR 15 June 2015, accepted 17 June 2015 (original submission 11 March 2015); expected doi:10.1002/2015JF003542

Subglacial hydrology and ice stream margin locations

Thibaut Perol,[1] James R. Rice[1,2], John D. Platt[1,3], Jenny Suckale[4]

Abstract. Fast flowing ice streams in West Antarctica are separated from the nearly stagnant ice in the adjacent ridge by zones of highly localized deformation known as shear margins. It is presently uncertain what mechanisms control the location of shear margins, and possibly allow them to migrate. In this paper we show how subglacial hydrological processes can select the shear margin location, leading to a smooth transition from a slipping to a locked bed at the base of an ice stream. Our study uses a two-dimensional thermo-mechanical model in a cross-section perpendicular to the direction of flow. We confirm that the intense straining at the shear margins can generate large temperate regions within the deforming ice. Assuming that the melt generated in the temperate ice collects in a drainage channel at the base of the margin, we show that a channel locally decreases the pore pressure in the subglacial till. Therefore the basal shear strength just outside the channel, assuming a Coulomb-plastic rheology, can be substantially higher than that inferred under the majority of the stream. Results show that the additional basal resistance produced by the channel lowers the stress concentrated on the locked portion of the bed. Matching the model to surface velocity data we find that shear margins are stable when the slipping-to-locked bed transition occurs less than 500 m away from a channel operating at an effective pressure of 200 kPa and for a hydraulic transmissivity equivalent to a basal water-film of order 0.2 mm thickness.

1. Introduction

The Siple Coast ice streams in West Antarctica are the major transport routes of ice into the Ross Ice Shelf [*Bamber et al.*, 2000]. These ice streams are of order 1 km thick, hundreds of kilometers long, 30 to 80 km wide and flow at hundreds of $\mathrm{m\,yr^{-1}}$. Ice streams are separated by a ridge of stagnant ice, which flows 2 to 3 orders of magnitude slower than the ice stream [*Shabtaie and Bentley*, 1987]. The boundary between a nearly stagnant ridge, locked at its base, and an ice stream that slips on the bed is called a shear margin. Shear margins migrate both away and towards the center of the ice stream [*Bindschadler and Vornberger*, 1998; *Echelmeyer and Harrison*, 1999; *Clarke et al.*, 2000]. However, the mechanisms that control their locations are still uncertain. In this paper we investigate the role subglacial hydrological processes may have in selecting the shear margin locations.

Ice streams flow in response to a small surface slope ($\sim 1.3\times10^{-3}$) [*Joughin et al.*, 2002], which corresponds to a gravitational driving shear stress of $\sim$ 10 kPa. This driving stress is balanced by a combination of basal drag beneath the ice stream and lateral drag at its shear margins [*Whillans and Van Der Veen*, 1993]. The high pore pressure in the underlying sediments, which is almost equal to the ice overburden pressure, leads to an extremely low yield strength ($\sim$ 1 to 5 kPa) of the plastically deforming till [*Engelhardt and Kamb*, 1997; *Kamb*, 2001]. A force balance, neglecting gradients in longitudinal stress [*Whillans and Van der Veen*, 1997], shows that the majority of the gravitational driving stress is supported by lateral drag at the shear margin [*Joughin et al.*, 2002].

Previous modeling studies have shown that the intense frictional heating at the shear margin can lead to the formation of temperate ice within the margin [*Jacobson and Raymond*, 1998; *Perol and Rice*, 2011; *Schoof*, 2012; *Suckale et al.*, 2014; *Perol and Rice*, 2015]. From a physically-derived triple-valued relation between the lateral drag and the shear strain rate, *Perol and Rice* [2015] found that for the shear strain rates measured at the margins of West Antarctic ice streams – sufficiently high for development of temperate ice within the margins – the calculated lateral drag generally lies along the low strength valley of the curve showing that triple-valued relation. Therefore the coupling between large strain rates and the presence of temperate ice can weaken the shear margin. A force balance predicts that the reduction of lateral drag implies that the basal yield strength must be enhanced in the margin near the transition from a slipping to a locked bed to prevent the runaway growth of the slipping portion of the ice stream bed towards the ridge. *Jacobson and Raymond* [1998], *Schoof* [2004] and *Schoof* [2012] also found that the basal yield strength must increase within the shear margin to prevent margin migration. They link the transition from a slipping to a locked bed to the large increase in till strength expected to occur at the onset of basal freezing. This concept of limiting the slipping zone width by locally enhanced resistance is analogous to the cohesive zone concepts developed in fracture mechanics – sometimes known as Barenblatt-Dugdale cohesive zone models [*Barenblatt*, 1959; *Dugdale*, 1960; *Bilby et al.*, 1963], also formulated for non-linear rheologies [*Rice*, 1968a, b].

While *Jacobson and Raymond* [1998], *Schoof* [2004] and *Schoof* [2012] associated basal strengthening to freezing of the bed, we investigate here the hypothesis, formulated in *Perol and Rice* [2011, 2015], that the shear margin location is controlled by the presence of a drainage channel at the base of the shear margin. Our hypothesis is supported by the observation of a cavity filled with flowing water between the bottom of the ice sheet and the bed at the margin of Kamb ice stream [*Vogel et al.*, 2005]. Extending these

[1]School of Engineering and Applied Sciences, Harvard University, Cambridge, MA, USA.
[2]Department of Earth and Planetary Sciences, Harvard University, Cambridge, MA, USA.
[3]Now at the Department of Terrestrial Magnetism, Carnegie Institution for Science, Washington, DC, USA.
[4]Department of Geophysics, Stanford University, Palo Alto, CA, USA.

0148-0227/15/$9.00

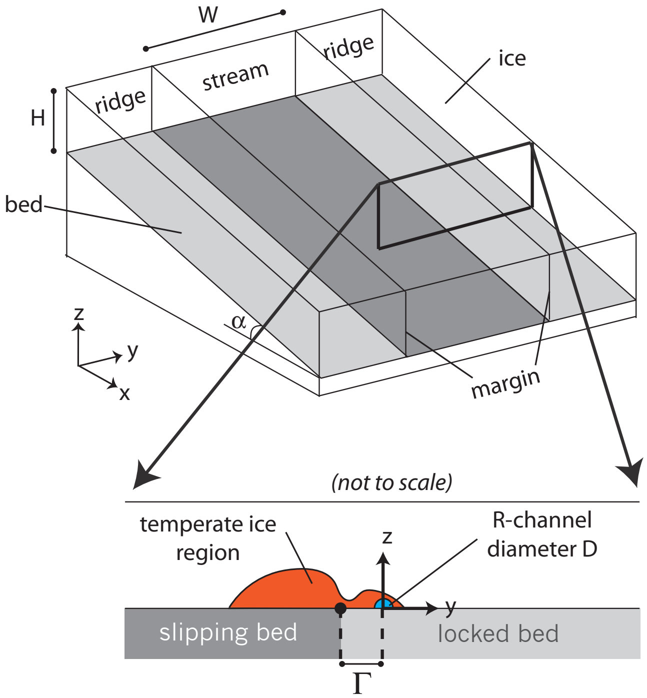

Figure 1. A sketch of the geometry assumed in our model. The ice thickness is H and the ice stream width is W. An R-channel of diameter $D = 1$ m located at $y = 0$ collects the meltwater generated inside the temperate ice region. The slipping-to-locked bed transition at $y = -\Gamma$ is chosen so that the basal shear stress is (1) non-singular at the transition, (2) equal to the yield strength where there is slipping, and (3) below the yield strength where there is locking. The two-dimensional cross-section is equivalent to the three-dimensional geometry assuming no downstream variations.

concepts to a model that couples ice flow to the underlying subglacial hydrology, we show that the decreased pore pressures near the channel strengthen the bed, and may allow for a smooth transition from a slipping to a locked bed. All calculations in this paper are done for the well studied Dragon margin of Whillans ice stream B2. Nonetheless, it is plausible that our conclusions extend to all Siple Coast ice streams that experience high enough strain rates within the shear margins for significant temperate zones, hence melt generation, to occur.

We derive a two-dimensional model for the steady-state flow of an ice stream and the adjacent ridge assuming that the bed is slipping beneath the ice stream and locked beneath the ridge. The mechanical model is coupled to a thermal model of the shear margin using the temperature-dependent Glen's law with the parameterization summarized by *Cuffey and Paterson* [2010]. A simple hydrological model based on a channel located within the shear margin is used to predict how the yield strength varies beneath the ice stream, assuming that the till is a Coulomb-plastic material [*Tulaczyk et al.*, 2000]. Our model can be thought of as an extension of the model used by *Suckale et al.* [2014] that adds the coupling with subglacial hydrological processes to fully determine the basal strength distribution, rather than assuming a uniform strength. The governing equations are solved numerically using the finite element package COMSOL. To begin we derive the equations for the mechanical, thermal and hydrological model in Section 2. We then develop the analogy with fracture mechanics in Section 3. In Section 4, we show that a realistic yield strength profile under the stream reduces the stress concentrated on the locked bed beneath the ridge. Finally, we discuss supporting observations and limitations of the model in Section 5.

2. Model

Our model uses the same two-dimensional geometry as *Suckale et al.* [2014]. The work presented in this paper is consistent with the results of *Suckale et al.* [2014] and shows that in order to fit the Dragon margin deformation data, a region of temperate ice is required at the margin. Figure 1 shows a schematic of the temperate zone for Dragon margin, based on shapes determined in our simulations here, with the addition of a semi-circular Röthlisberger channel (R-channel) of diameter $D = 1$ m incised into the ice at the base of the shear margin to drain the meltwater produced. Such assumptions are compatible with the observations mentioned by *Vogel et al.* [2005] at the margin of Kamb ice stream (details in the discussion section). We define x as the coordinate parallel to the direction of downstream flow, y as the horizontal coordinate perpendicular to the shear margin such that $y = 0$ coincides with the center of the channel, and the vertical coordinate z is taken positive upward from the base of the ice. The slipping-to-locked bed transition occurs at a distance Γ from the channel center, and thus the bed is slipping for $y < -\Gamma$ and locked for $y > -\Gamma$. We refer to this location as the locking point in this paper. The ice stream center is located at $y = -W/2$, where W is the width of the ice stream, and we neglect any variations of ice thickness in the direction perpendicular to the downstream ice flow. Based on the InSAR observations from *Joughin et al.* [2002] we choose $W = 34$ km.

2.1. Mechanical model

We define the velocity vector such that (u, v, w) are components in the (x, y, z) directions. Fast ice flow in the downstream direction is resisted by basal and lateral shear stresses. The in-plane strain rate components $\dot\epsilon_{yy}$, $\dot\epsilon_{yz}$, and $\dot\epsilon_{zz}$, oriented perpendicular to motion, are typically at least two orders of magnitudes lower than the anti-plane strain rates $\dot\epsilon_{yx}$ and $\dot\epsilon_{zx}$ [*Echelmeyer and Harrison*, 1999], and thus we neglect their contributions to the ice viscosity. This allows us to simplify the x-direction force balance to that of an anti-plane shear flow of local velocity $u = u(y, z)$ driven by gravity,

$$\frac{\partial}{\partial y}\left(\mu(\dot\epsilon_E, T)\frac{\partial u}{\partial y}\right) + \frac{\partial}{\partial z}\left(\mu(\dot\epsilon_E, T)\frac{\partial u}{\partial z}\right) + \rho_{ice} g \sin\alpha = 0. \tag{1}$$

We call μ the temperature and strain rate dependent dynamic viscosity, and $\dot\epsilon_E$ is the second invariant of the strain rate tensor, $\dot\epsilon_E = \sqrt{\dot\epsilon_{ij}\dot\epsilon_{ij}/2} = |\nabla u|/2$. The ice stream flows in response to the gravitational driving stress $\tau_{grav} = \rho_{ice} g H \sin\alpha$ where $\rho_{ice} = 910$ kg.m^{-3} is the ice density, $g = 9.8$ m.s^{-2} is the acceleration due to gravity, $H = 1$ km is the ice sheet thickness – a reasonable width-averaged value in the Dragon margin region [*Harrison et al.*, 1998; *Joughin et al.*, 2002] – and $\sin\alpha = 1.2 \times 10^{-3}$ is the absolute value of the surface slope of the ice stream [*Joughin et al.*, 2002].

Ice can deform through several mechanisms linked to different physical phenomena such as dislocation motion and the diffusion of atoms. The dominant deformation mechanism varies with stress and temperature. Diffusional creep is expected to dominate at low stress and can be modeled by *Frost and Ashby* [1982]

$$(\dot\epsilon_D)_{ij} = \frac{42\Omega}{k_B T d_g^2} B \exp\left(-\frac{Q}{RT}\right)\tau_{ij} \equiv \frac{1}{2\eta(T)}\tau_{ij}. \tag{2}$$

Table 1. Parameter values for the two deformation mechanisms considered in this study. Diffusional creep and Glen's law are modeled using parametrization from respectively *Frost and Ashby* [1982] and *Cuffey and Paterson* [2010].

Parameter	notation	[units]	values
Diffusional creep			
Molecular volume	Ω	[m^3]	$3.27.10^{-29}$
Boltzman constant	k_B	[m^2 kg s^{-2} K^{-1}]	$1.38.10^{-23}$
Grain size	d_g	[mm]	1
Pre-factor	B	[m^2 s^{-1}]	$9.1.10^{-4}$
Activation energy	Q	[kJ mol^{-1}]	59.4
Gas constant	R	[J.K^{-1} mol^{-1}]	8.314
Glen's law			
Pre-factor	A^*	[s^{-1} Pa^{-3}]	3.5×10^{-25}
Gas constant	R	[J.K^{-1} mol^{-1}]	8.314
Pre-melting temperature	T^*	[K]	263.15
Activation energy when $T < T^*$	Q_c	[kJ mol^{-1}]	60
Activation energy when $T \geq T^*$	Q_c	[kJ mol^{-1}]	115

Parameter values are taken from *Frost and Ashby* [1982] and written explicitly in Table 1. At higher stresses the deformation is assumed to follow Glen's law [*Cuffey and Paterson*, 2010],

$$(\dot{\epsilon}_G)_{ij} = A^* \exp\left[-\frac{Q_c}{R}\left(\frac{1}{T} - \frac{1}{T^*}\right)\right] \tau_E^2\, \tau_{ij} \equiv A(T)\, \tau_E^2\, \tau_{ij} \quad (3)$$

The temperature dependence of Glen's law is modeled using the function proposed by *Cuffey and Paterson* [2010] (page 72) and the parameter values are written in Table 1. We use $\tau_E^2 = \tau_{ij}\tau_{ij}/2 = (\tau_{xy}^2 + \tau_{xz}^2)$ to denote the second invariant of the deviatoric stress tensor. Here we have neglected important physical effects such as the dependence of A on the melt fraction or grain size of the ice, or the possibility that, for the large shear stress expected to occur near any abrupt transition from a slipping to a locked bed, the dislocation creep rheology with $n = 4$ from *Durham et al.* [1997] will be the dominant deformation mechanism.

We assume that for all stresses and temperatures the strain rate is equal to that of the faster operating deformation mechanism, allowing us to write

$$\dot{\epsilon} = \max(\dot{\epsilon}_{\mathbf{D}}, \dot{\epsilon}_{\mathbf{G}}). \quad (4)$$

Equation (4) leads to a formula for the ice viscosity

$$\mu = \min\left(\eta(T), [2A(T)]^{-1/3} \,|\nabla u|^{-2/3}\right). \quad (5)$$

Accounting for diffusional creep alongside Glen's law provides a more realistic description of ice deformation and prevents the ice viscosity from diverging when the stresses are small. In practice the linear rheology is only dominant at the surface of the ice in the center of the stream and in the center of the ridge where the two traction free boundaries meet. Most of the ice deforms following Glen's law.

Next we discuss the mechanical boundary conditions for our model. Under the ice stream where the bed is slipping the stress τ_{xz} on the bed must be equal to the yield strength of the till. Assuming that the yield strength of the plastically deforming till is proportional to the difference between the normal stress and the pore pressure [*Tulaczyk et al.*, 2000], we find the strength profile from the basal pore pressure profile solved by the hydrological model developed in Section 2.3. Under the ridge the bed is locked and we have a no slip boundary condition. The boundary conditions at the base of the ice of the mechanical model are

$$\tau_{xz} = \tau_{yield}(y) \qquad \text{for } y \leq -\Gamma, z = 0 \quad (6)$$

$$u = 0 \qquad \text{for } y > -\Gamma, z = 0. \quad (7)$$

The ice sheet surface, at $z = H$, and channel wall are traction free. On the sides of the computational domain we impose the symmetric boundary conditions used by *Suckale et al.* [2014].

Note that we do not assume that the slipping-to-locked bed transition occurs at the point where the bed freezes, as in the model of *Schoof* [2012]. In our simulations the transition from temperate to frozen bed occurs further into the ridge ($y > -\Gamma$) due to the development of a zone of temperate ice around the locking point (see Figure 1).

2.2. Thermal model

Following *Suckale et al.* [2014] we solve the steady-state heat equation within the ice

$$\frac{\partial}{\partial y}\left(K\frac{\partial T}{\partial y}\right) + \frac{\partial}{\partial z}\left(K\frac{\partial T}{\partial z}\right) - \rho_{ice}C_{ice}\left(v\frac{\partial T}{\partial y} + w\frac{\partial T}{\partial z}\right) + \left[1 - \hat{H}(T - T_{melt})\right] 2\tau_E\dot{\epsilon}_E = 0, \quad (8)$$

where $\hat{H}$ is the Heaviside function. We assume that all the shear heating in the temperate ice is absorbed as latent heat to generate meltwater. The conversion of frictional heating into latent heat caps the temperature at the melting point. We account for the changes in the thermal conductivity K and specific heat capacity C_{ice} of the ice with temperature in our model following *Cuffey and Paterson* [2010] (page 400).

We use the vertical advection profile suggested by *Zotikov* [1986],

$$w(y, z) = -a\frac{z}{H}, \quad (9)$$

where a is the accumulation rate at the surface. We choose $a = 0.1$ m yr^{-1}, a reasonable value for the Siple Coast ice stream region according to *Giovinetto and Zwally* [2000] and *Spikes et al.* [2004]. *Suckale et al.* [2014] highlighted the important role horizontal advection plays in the formation of temperate ice, with larger in-plane advection leading to less temperate ice. The horizontal advection component v in equation (8) is often modeled using the net margin migration (outward migration of the margin [*Echelmeyer et al.*, 1994; *Harrison et al.*, 1998] minus the influx of cold ice from the ridge into the margin [*Echelmeyer and Harrison*, 1999]). However, *Suckale et al.* [2014] showed that strong horizontal advection, which is modeled using the vertical shearing profiles from *Jacobson and Raymond* [1998], eliminates almost all of the temperate ice, making it impossible to closely match surface velocity measurements [*Echelmeyer et al.*, 1994; *Echelmeyer and Harrison*, 1999]. For this reason we choose to neglect lateral advection.

Following the observations presented by *Engelhardt* [2004] and *Vogel et al.* [2005], we assume that the slipping bed and the channel wall are at the pressure-dependent melting point $T_{melt} = -0.6°\mathrm{C}$ [*Hooke*, 2005]. Where the bed is locked the geothermal heat flux is chosen such that the ice temperature under the ridge and far from the shear margin is $-5°\mathrm{C}$ [*Rose*, 1979]. This leads to $G_{geo} \approx 70$ mW.m^{-2}, which is in agreement with observations in the Siple Coast region [*Engelhardt*, 2004; *Maule et al.*, 2005]. The yearly-averaged temperature at the surface of the ice sheet is $T_{atm} = -26°\mathrm{C}$ [*Joughin et al.*, 2002; *Engelhardt*, 2004]. As in the mechanical model, we assume symmetric boundary conditions at the sides of the computational domain.

2.3. Subglacial hydrological model and basal yield strength profile

We develop a model for the flow of subglacial water towards the channel operating at a reduced water pressure p_{ch} [*Röthlisberger*, 1972]. The hydrological model allows us to calculate the basal pore pressure profile and, hence, evaluate the yield strength profile $\tau_{yield}(y)$ of the slipping bed, used as a boundary condition in the mechanical model.

The heat balance at the ice-till interface can be written as

$$G_{geo} - G_{ice} + \tau_{yield}\, u_b = \rho_{ice} L w_m, \quad (10)$$

where $L = 335$ kJ kg^{-1} is the latent heat of fusion per unit mass, G_{ice} is the heat flux into the ice at the base of the ice sheet, $u_b(y) = u(y, z = 0)$ is the ice velocity in the downstream direction at the base of the ice stream, and w_m is the basal melting rate in m s^{-1}. Here we have assumed that all frictional heating at the base of the ice stream is due to basal sliding, which generates heat at the rate $\tau_{xz}(y, z = 0)u_b(y) = \tau_{yield}(y)u_b(y)$. This means that we have ignored the heat generated by dissipation in the flowing water beneath the ice stream, which *Kyrke-Smith et al.* [2014] showed is likely a negligible source of heat.

Conservation of fluid mass accounting for basal melting at the ice-till interface leads to

$$\rho_w \nabla \cdot \mathbf{Q} = \rho_{ice} w_m, \quad (11)$$

where $\rho_w = 1000$ kg.m^3 is the density of water and $\mathbf{Q}$ is the water flow rate vector, parallel to the basal plane, in m^2/s. Using Darcy's law

$$\mathbf{Q} = -\frac{T_{wf}}{\rho_w g} \nabla (p + \rho_w g z), \quad (12)$$

where ∇ operates in the basal plane, T_{wf} is the hydraulic transmissivity of the subglacial drainage system, and p the local absolute pore pressure.

Treating T_{wf} as constant (i.e., independent of p) and combining equations (11) and (12), the basal melting rate becomes

$$w_m = -\frac{T_{wf}}{\rho_{ice} g} \nabla^2 (p + \rho_w g z). \quad (13)$$

Inserting this relation into equation (10) and assuming that the ice surface has a constant uniform downstream slope and no transverse slope (cf. Figure 1), and that the downstream pressure gradient is constant we obtain

$$G_{geo} - G_{ice} + \tau_{yield} u_b = -\frac{T_{wf} L}{g} \frac{\partial^2 p}{\partial y^2}. \quad (14)$$

Ignoring the variations of the normal stress applied to the bed in the channel vicinity [*Weertman*, 1972; *Röthlisberger*, 1972]

$$\tau_{yield}(y) = f[\sigma_0 - p(y)] + c, \quad (15)$$

where $\sigma_0 = \rho_{ice} g H$ is the ice overburden pressure at the bed. We assume a till friction coefficient of $f = 0.5$ [*Rathbun et al.*, 2008] and a till cohesion of 1 kPa [*Kamb*, 2001]. Therefore the basal yield strength for $y < -D/2$ satisfies

$$G_{geo} - G_{ice} + \tau_{yield} u_b = \frac{T_{wf} L}{f\, g} \frac{\partial^2 \tau_{yield}}{\partial y^2}, \quad (16)$$

with $\tau_{yield}(y = -D/2) = f(\sigma_0 - p_{ch}) + c$ and $(\partial \tau_{yield}/\partial y) = 0$ at $y = -W/2$.

The yield strength of the locked bed ahead of the channel in the ridge ($y \geq D/2$), before reaching locations of frozen bed, is assumed uniform,

$$\tau_{yield} = f(\sigma_0 - p_{ch}) + c. \quad (17)$$

This formula assumes that the pore pressure is constant and equal to the channel water pressure for the few tens of meters immediately adjacent to the channel. Our simulations show that the pressure gradient predicted by the hydrological model is, indeed, negligible over this length scale for the typical transmissivity we infer (see Section 4.2).

3. Stable margin: a crack problem

As discussed by *Suckale et al.* [2014], a mathematical analogy can be drawn between an ice stream and an anti-plane fracture (a planar crack for which the only displacement is in the x-direction, parallel to the crack front, and

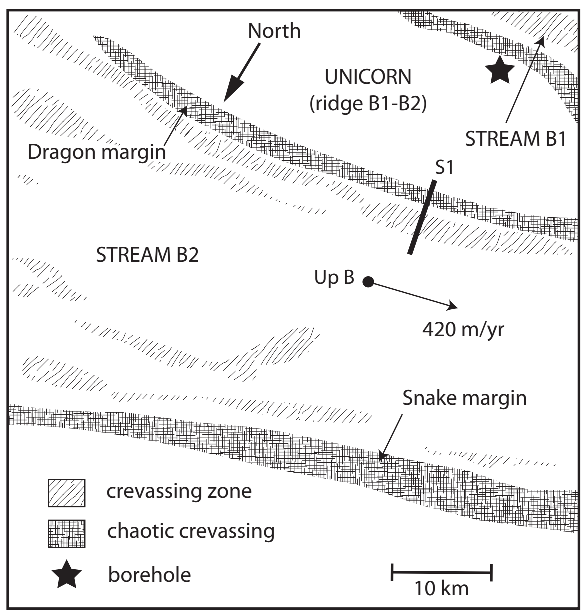

Figure 2. Location of 'S1' on Whillans ice stream B2 where *Echelmeyer et al.* [1994] measured a surface velocity profile to extract the Dragon margin shear strain rate profile. The black star at the interstream ridge between Whillans ice stream B1 and B2, an area commonly referred to as the Unicorn, indicates the location of a borehole drilled by a Caltech group (mentioned in a personal communication from H. Engelhardt by *Clarke et al.* [2000]). At Up B, the ice velocity is measured at 420 m yr^{-1}. North-South axis is approximately perpendicular to Dragon margin. This figure is redrawn and modified based on *Echelmeyer and Harrison* [1999].

varies spatially only with y and z) in a non-linear elastic material. In this analogy the downstream velocity corresponds to the anti-plane displacement, the slipping bed beneath the ice stream to the crack face, the locked bed beneath the ridge to the unfractured material ahead of the crack, and the transition from a slipping to a locked bed (at $y = -\Gamma$) to the crack tip. This analogy tells us that the ice stream will concentrate large stresses on the locked bed, as shown analytically for a Newtonian rheology [*Schoof*, 2004, 2012] and numerically for more realistic ice rheologies [*Jacobson and Raymond*, 1998; *Suckale et al.*, 2014]. From this we conclude that for a stable margin configuration – where the shear stress resolved on the bed is always less than the yield strength of the till when the bed is locked – to exist there must be a mechanism that greatly strengthens the bed within the shear margin. If no such strengthening mechanism exists then the locked bed will yield and the ice stream will widen.

One possible mechanism studied in *Jacobson and Raymond* [1998] and *Schoof* [2012] linked the strengthening to freezing of the bed. Taking a different approach, we show here that a channel at the base of the shear margin can limit the maximum stress acting on the locked bed. That occurs by increasing the basal resistance over a kilometers wide zone in the shear margin. This occurs because the channel operates at a lower water pressure, and thus lowers the pore pressure in the till in the immediate vicinity of the channel. Combining the higher effective normal stress associated with this decreased pore pressure with the Coulomb-plastic rheology for the yield strength, we see that the yield strength of the bed will increase from the center of the stream to the margin. This increased basal resistance is similar to the Barenblatt-Dugdale cohesive zone models commonly used in fracture mechanics [*Barenblatt*, 1959; *Dugdale*, 1960; *Bilby et al.*, 1963], and alleviates some of the stress concentration (a stress singularity for the mathematical model of a planar crack with a sharp tip) created by the transition from a slipping to a locked bed.

4. Results

The channel diameter is fixed at $D = 1$ m and the effective stress in the channel at $(\sigma_0 - p_{ch}) = 200$ kPa. These values are consistent with estimates of the channel radius and effective pressure of a steady state R-channel collecting the meltwater generated in the temperate ice region (see details in Appendix A). Next to the channel the mesh is refined with elements as small as 1 mm. The code is benchmarked against the solutions for the stress field near the transition from a slipping to a locked bed developed for isothermal ice conditions by *Suckale et al.* [2014].

To constrain our model we match the downstream velocity profile 'S1' measured at the surface of Dragon margin [*Echelmeyer et al.*, 1994; *Echelmeyer and Harrison*, 1999], which is the southern margin of Whillans ice stream B2 (see Figure 2). This velocity profile is one of the few concrete observations available in this area, which is difficult to access due to the extensive surface crevassing [*Harrison et al.*, 1998]. We vary G_{ice} to match our model to this data. A typical value leading to good agreement with the data is $G_{ice} \approx 100\,\mathrm{mW.m}^2$. This changes the basal shear strength under the stream far away from the channel, with typical values of 1.8 to 2.2 kPa, in agreement with the measurements [*Kamb*, 2001] and previous modeling studies by *Joughin et al.* [2004] and *Suckale et al.* [2014].

The till itself is of very low hydraulic conductivity (10^{-10} $\mathrm{m\,s^{-1}}$, cf. *Tulaczyk et al.* [2000]). In this paper, we assume that all seepage takes place close to and, essentially, along the ice-till interface like in, e.g., *Weertman* [1972], *Creyts and Schoof* [2009], *Le Brocq et al.* [2009] and *Kyrke-Smith et al.* [2014]. Our results for T_{wf} are interpreted in terms of an equivalent water film thickness h satisfying

$$T_{wf} = (h^3 \rho_w g)/(12\mu_w), \quad (18)$$

corresponding to a Hele-Shaw type of Poiseuille flow between two plates separated by a distance h. However, the model is valid for any distributed drainage system satisfying Darcy's law (e.g., linked cavities [*Hewitt*, 2011]), and h is just a simple proxy for T_{wf} of that system.

4.1. Unstable margin locations

First we assume the locking point coincides with the center of the channel by setting $\Gamma = 0$ and assume that the bed is slipping for $y < -D/2$ and locked for $y > D/2$ like in *Suckale et al.* [2014]. Without the subglacial hydrological model (i.e., ignoring basal strengthening of the slipping bed) and assuming a uniform low basal yield strength of 2.56 kPa under the ice stream to fit the surface deformation data, the basal shear stress acting on the locked bed (solid blue line in Figure 3) is approximately six times higher than the yield strength of the locked bed (dashed black line in Figure 3).

We include the subglacial hydrological model from Section 2.3 and investigate how the decreased pore pressure associated with the channel alters the stress resolved on the locked bed. Our simulations show that for small values of h, corresponding to a low transmissivity of the hydrological system, the pore pressure under the stream bed is high. This implies a low yield strength of the slipping bed, leading to a minimal reduction in the shear stress acting on the locked bed in the immediate vicinity of the channel (cf. Figure 4). Increasing the transmissivity increases the width over which the strength of the slipping bed is large and leads to a larger reduction of the shear stress on the locked bed at $y = D/2$ (see Figure 4). This is in agreement with standard cohesive zone concept of fracture mechanics [*Barenblatt*, 1959; *Dugdale*, 1960; *Bilby et al.*, 1963]. We find that a water thickness of $h = 0.105$ mm, equivalent to a transmissivity of 5.2×10^{-7} $\mathrm{m^2\,s^{-1}}$, decreases the maximum shear stress acting on the locked bed at the channel wall by a factor 4.5 compared with the simulation for a constant $\tau_{yield} = 2.56$

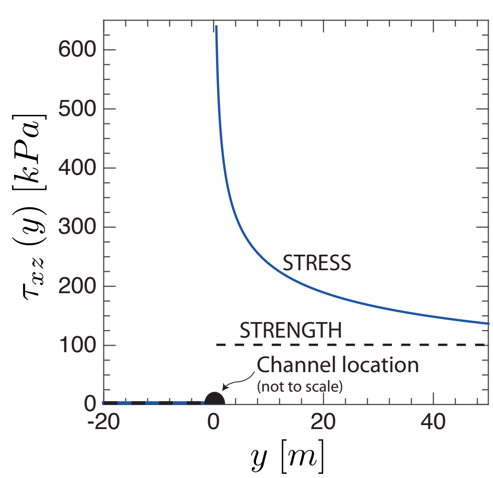

Figure 3. Simulation when the locking point coincides with the channel center ($\Gamma = 0$), without the subglacial hydrological model and for a locked bed when $y > D/2$. The yield strength of the slipping bed ($y < -D/2$) is uniform and low, $\tau_{yield} = 2.56$ kPa. The solid line and dashed line are respectively the basal shear stress and the bed yield strength.

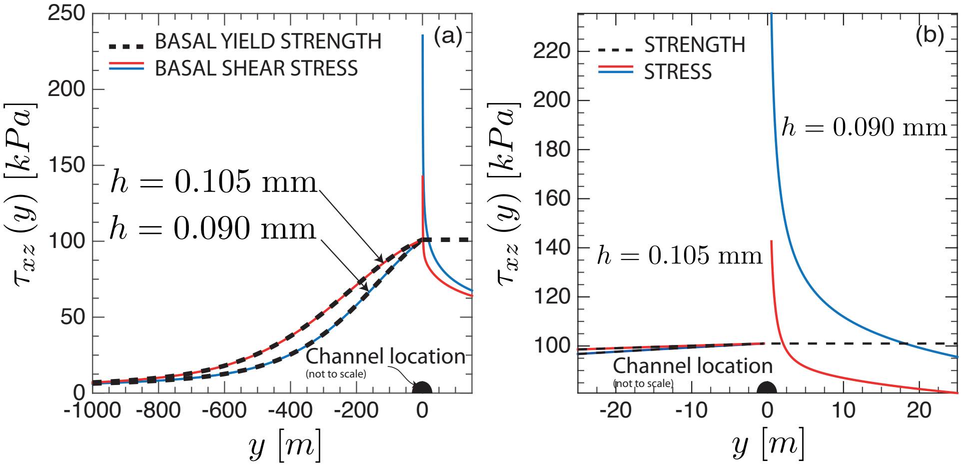

Figure 4. Simulations when the locking point coincides with the channel center ($\Gamma = 0$), with the subglacial hydrological model, and a locked bed when $y > D/2$. (a) The basal shear stress profiles (solid lines) and yield strength profile (dashed line) for various values of h. (b) Blow-up of (a) in the vicinity of the channel.

kPa (like in Figure 3). The thicknesses of the water film inverted for here are smaller than the ones inferred by *Kamb* [2001] and we discuss these discrepancies in the discussion section. For $h > 0.105$ mm the simulations show unphysical basal back sliding of the slipping bed. Therefore, when the margin is collocated with the channel, the associated transmissivity reaches a maximum corresponding to $h = 0.105$ mm that leads to a shear stress larger than the strength on the locked bed – this is an unstable margin configuration.

4.2. Stable margin locations

Now we fix the locking point at a distance Γ from the center of the channel (cf. Figure 1) and vary the transmissivity to find the value that allows for a non-singular basal shear stress profile. Equivalently we can fix the transmissivity and find the value of Γ that allows for a smooth transition from a slipping-to-locked bed. When the locking point is 50 m away from the channel center ($\Gamma = 50$ m) we find the best agreement with the surface deformation data (Figure 5) occurs for a yield strength far away from the channel of 2.0 kPa. The basal shear stress profile is non-singular for $h = 0.114$ mm, which is equivalent to $T_{wf} = 6.7 \times 10^{-7}$ $\mathrm{m^2\,s^{-1}}$. The intense shear heating at the transition from a slipping to a locked bed leads to the formation of a temperate ice zone (see Figure 5), as predicted by *Jacobson and Raymond* [1998], *Schoof* [2012] and *Suckale et al.* [2014]. The formation of temperate ice localizes deformation to a narrow band at the margin and is required to fit the surface velocity profile from *Echelmeyer et al.* [1994].

The basal shear stress profile $\tau_{xz}(y, z = 0)$ (solid gray curve) and the yield strength profile $\tau_{yield}(y)$ (dashed black line) in this simulation are shown in Figure 6. As predicted by standard Barenblatt-Dugdale cohesive zone concept [*Barenblatt*, 1959; *Dugdale*, 1960; *Bilby et al.*, 1963], bed strengthening in the vicinity of the locking point – where the yield strength is approximately fifty times higher than in the center of the stream – eliminates the singularity from the basal shear stress and creates a smooth continuation of the stress at the locking point. As we approach the traction free channel the basal shear stress increases and eventually becomes larger than the basal strength for a few meters on both sides of the channel. This scenario would apparently imply an unstable margin when $\Gamma = 50\,\mathrm{m}$, although we subsequently show that a stable configuration can exist in that case.

Next we move the locking point further from the channel. The strength profiles (dashed black lines) and the stress profiles (red and blue solid lines for respectively $\Gamma = 200$ m and $\Gamma = 500$ m) are displayed in Figure 6. As before, the surface velocity profiles agree well with the ice deformation data (see Figure 7 for $\Gamma = 500$ m). The temperate ice zone still extends over ≈ 400 m above the bed and is 3 km wide. We find, for $\Gamma > 200$ m, basal shear stress profiles that are free of singularity and lower than the strength everywhere on the locked bed, corresponding to stable margin configurations. The width over which the bed strengthens increases with the hydraulic transmissivity. For $\Gamma = 50$ m the smooth transition occurs for a water film h of 0.114 mm thickness (equivalent to $T_{wf} = 6.7 \times 10^{7}$ $\mathrm{m^2\,s^{-1}}$), corresponding to basal yield strength higher than the gravitational driving stress over 1 km at the margin. For $\Gamma = 500$ m the basal

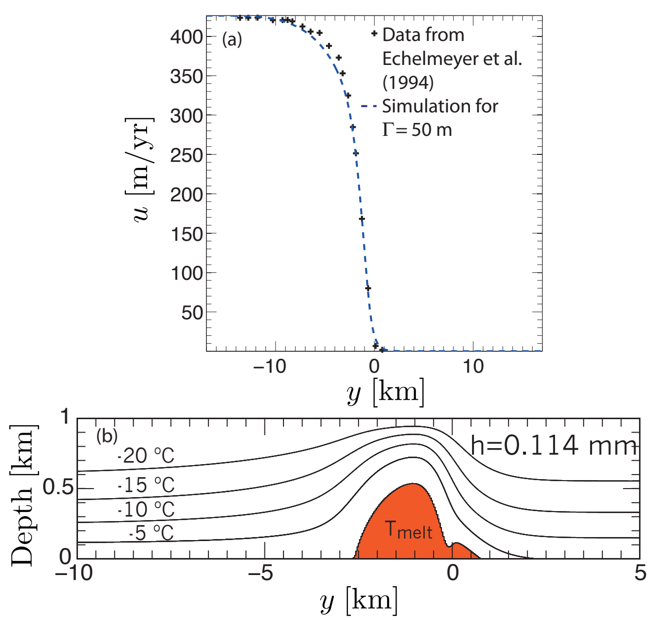

Figure 5. Results for a locking point 50 m away from the channel ($\Gamma = 50$ m). (a) Numerical surface velocities plotted alongside the data from *Echelmeyer et al.* [1994]. (b) Temperature field. In red is the temperate ice zone in which the temperature is capped at the melting point. The basal shear stress is free of singularity for $h = 0.114$ mm.

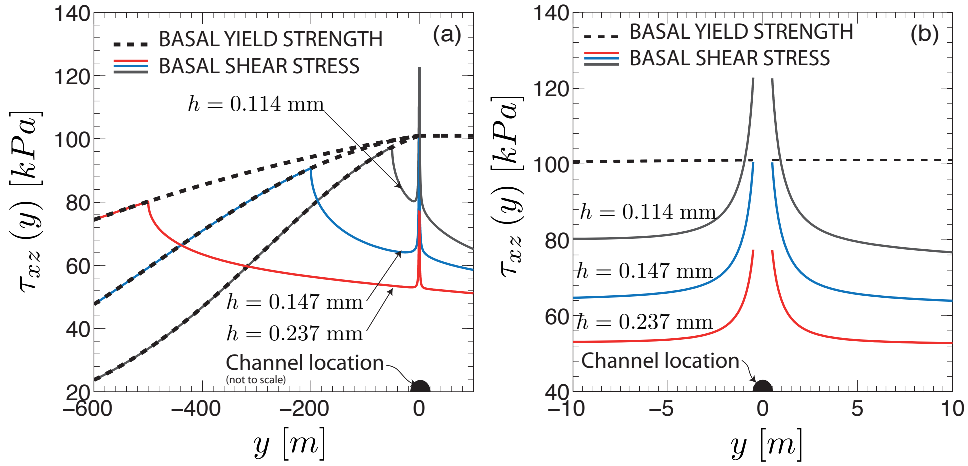

Figure 6. Basal yield strength and basal shear stress profiles predicted by the model. (a) Simulations for locking points located 50 m, 200 m and 500 m away from the center of the channel. The solid lines correspond to the shear stress profiles and the dashed lines to the strength profiles. The stress and the strength are equal where the bed is slipping. The margin is stable when the stress on the locked bed is lower than the yield strength. (b) Blow-up of (a) in the vicinity of the channel.

shear stress profile is non-singular for $h = 0.237$ mm (equivalent to $T_{wf} = 6.0 \times 10^{-6}$ m^2 s^{-1}) and corresponds to a basal strengthening over 2 km – with a yield strength at the locking point forty times higher than in the center of the ice stream.

We can use the results shown in Figure 6 to demonstrate that the hydraulic gradient ($\partial p/\partial y$) is small over the first few tens of meters immediately adjacent to the channel. Our simulations show that the basal pore pressure decreases from the channel pressure by 0.3% over 10 m and 3% over 100 m for $(\sigma_0 - p_{ch}) = 200$ kPa and $\Gamma = 500$ m. This means that, in the immediate vicinity of the channel, the pore pressure can be treated as uniform. Ignoring the changes in normal stress acting on the bed associated with the presence of a channel [*Nye*, 1953; *Röthlisberger*, 1972; *Weertman*, 1972] and other physical processes such as penetration of ice into underlying till [*Rempel*, 2008, 2009] and coupling between ice and till deformation [*Ng*, 2000], we therefore assume a constant yield strength in the first few meters ahead of the channel ($y > D/2$), as shown in equation (17).

As shown above, for $\Gamma < 50$ m the margin is apparently unstable because the stress is higher than the strength on both channel sides. However, allowing two 1.5 m wide slipping patches to form on both sides of the channel (see Figure 8), in the spirit of Barenblatt-Dugdale yielding zones, we find a stable margin configuration, so that the $\Gamma = 50$ m case is actually stable.

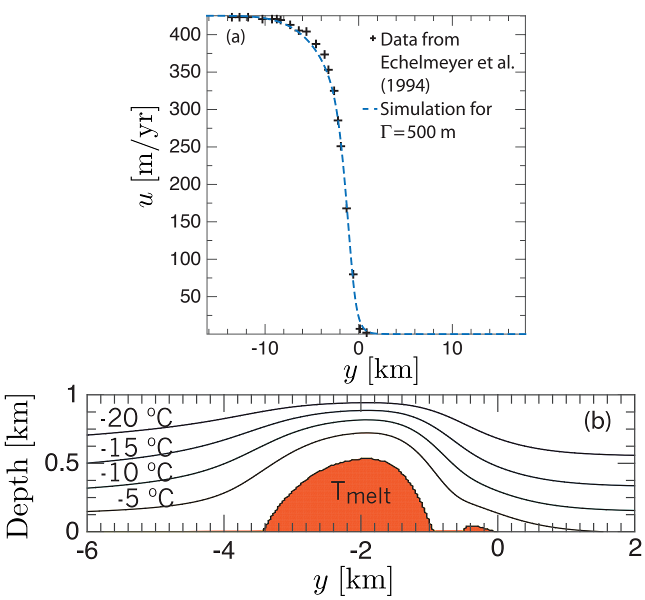

Figure 7. Results for a locking point 500 m away from the channel ($\Gamma = 500$ m). (a) Numerical surface velocities compare with data from *Echelmeyer et al.* [1994]. (b) Temperature field. In red is the temperate ice zone in which the temperature is capped at the melting point. The basal shear stress is free of singularity for $h = 0.237$ mm.

4.3. Stability diagram of an ice stream margin

The system has two main parameters: the locking point distance Γ from the channel center (the distance of the margin to the channel center) and the transmissivity T_{wf} of the subglacial hydrological system (equivalently, the water

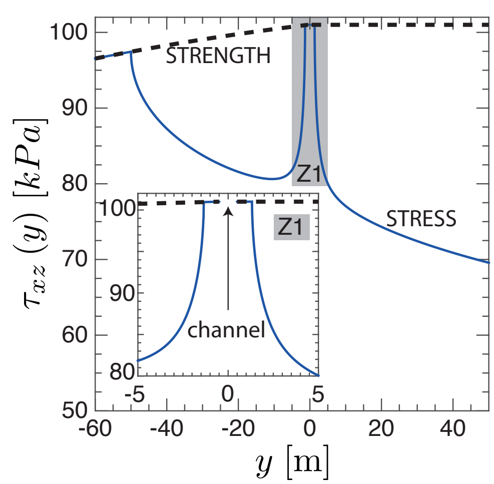

Figure 8. Stable margin configuration allowing for two slipping patches of 1.5 m width to develop on both sides of the channel located at $y = 0$. The margin is located at $\Gamma = 50$ m away from the channel center.

film thickness h). Varying these parameters in turn we can determine when the shear margin is stable. This leads to the stability diagram constructed in Figure 9 for an effective pressure in the channel of 200 kPa. Consider the point A for which the margin is stable when located 220 m away from the channel center, corresponding to $h = 0.15$ mm. A small increase of the hydraulic transmissivity to a value corresponding to $h = 0.18$ mm implies a migration of the margin (i.e., migration of the locking point) towards the center of the ice stream by 100 m – it is an inward migration. The next stable margin position is point B in Figure 9. If the transmissivity decreases to the initial value corresponding to $h = 0.15$ mm the margin migrates outwards by 100 m to retrieve the stable configuration indicated by point A in the stability diagram. The black crosses in this diagram correspond to simulations performed. For $\Gamma > 500$ m the black line transitions into the dashed line when the region of temperate ice no longer encompasses the channel, and thus our model is no longer valid. For small Γ the solid line transitions into a dashed line because stable margin configurations are expected to occur by developing slipping patches on both sides of the channel.

5. Discussion

5.1. Possible evidence for temperate ice and drainage channel at margin

Observational evidence indicates that temperate ice and/or a subglacial channel may exist within a shear margin. *Clarke et al.* [2000] used a high power radar system to image the entire thickness of the Unicorn (Ridge B1-B2) ice sheet. They made profiles in multiple directions and found numerous linear diffractors near the base of the ice sheet. One special feature that was recognized is the occurrence of diffractors 230 m above the bed, following what they called the 'Fishhook', a surface lineation observed in satellite imagery running parallel to the northern margin of Whillans

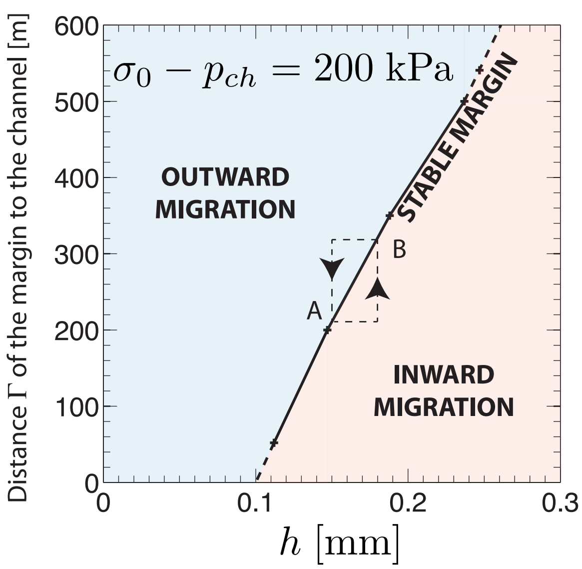

Figure 9. Stability diagram of an ice stream margin. Along the solid black line the margin is stable i.e., the basal shear stress is non-singular and the basal shear stress is lower than the yield strength on the locked bed. When the hydraulic transmissivity corresponding to a water film of thickness h is higher than predicted by the stable line the margin (the locking point) migrates inward i.e., towards the centerline of the ice stream. When h is lower the margin migrates outward, towards the ridge.

ice stream B1 and located in the middle of Unicorn. *Clarke et al.* [2000] suggested that one possible explanation for these features is that they reflect a zone of temperate ice that marks the inner boundary of an abandoned shear margin, while the outer boundary is marked by a band of crevasses that used to form the outer boundary of Dragon margin. This supports arguments presented by *Jacobson and Raymond* [1998], *Schoof* [2012] and *Suckale et al.* [2014] for the existence of temperate ice over a substantial fraction of the sheet thickness at a shear margin.

Clarke et al. [2000] also noted that a Caltech group had drilled into the ice at Unicorn approximately 1 km from the outer boundary of the northern margin of Whillans ice stream B1 (see Figure 2). They reported that, at approximately 56 m above the bed, the drill began encountering abnormal resistance. The penetration rate slowed within layers at 56-49 m, 44-22 m, and 14-0 m above the bed and some fresh scratches were observed on the the metal drill tip once back at the surface. They argue that these observations are strongly suggestive of entrained morainal debris. One of the possible mechanisms of formation of this debris is meltwater processes depositing sediment over a long period of time. Perhaps this morainal debris is a result of a channel development at the bed of the abandoned northern shear margin of Whillans ice stream B1.

Evidence for a channel was found when a borehole was drilled at one shear margin of Kamb ice stream, an ice stream on the Siple Coast that stopped flowing approximately 150 years ago [*Smith et al.*, 2002]. *Vogel et al.* [2005] drilled to the bottom of the ice sheet at the transition from the active upper part of Kamb ice stream to the stopped main trunk where the center stream velocity is 25 $\mathrm{m\,yr^{-1}}$. The borehole intersected a 1.6 m tall water-filled cavity between the bottom of the ice and the bed, a size comparable to our rough estimate for the diameter of a semi-circular channel collecting water from 100 km upstream at Dragon margin (cf. Appendix A). Additionally, videos from the bottom of this borehole showed horizontal advection of small solid particles sinking into the cavity, indicating a still active flow of water within the cavity (the direction of flow was not reported). They estimated that the shear margin reconnected to the basal hydrological system about 60 years ago, and argued that the formation of this 1.6 m tall water-filled cavity is associated with the re-supply of basal water from areas of basal melting further upstream. This raises the possibility that the borehole fortuitously encountered a channel of the type that we conjecture. At least, it shows that channelized transport beneath an ice stream margin is a realistic possibility and implies that a source of liquid water must exist near this shear margin.

5.2. Water film thickness

In our model we assumed a constant water film thickness under the ice stream. A better model would incorporate how h increases as the effective pressure at the base of the ice stream decreases. However, this is difficult due to the current uncertainty surrounding the appropriate parameterization for the dependence of h on effective pressure. *Engelhardt and Kamb* [1997] and *Kamb* [2001] found that $h = 2$ mm fits the borehole inflow/outflow observations at the bed of Whillans ice stream B2. However, the typical effective pressures in these measurements were in the range of 20 to 60 kPa (specifically ≈ 20 kPa for Kamb ice stream stream, 40 kPa for Bindschadler ice stream, and 60 kPa for Whillans ice stream). The hydraulic conductivity of the subglacial hydrological system is found to be extremely sensitive to changes in effective pressure. Also, measurable flow on the time scales they studied typically required an initial overpressure to hydraulically fracture the ice from the bed before measurable transport was detected. Our own and *Suckale et al.* [2014] estimates of τ_{yield} in the center of the stream (interpreted as $f(\sigma_0 - p) + c$) to fit the deformation data also suggest low effective pressures of order 10 kPa for Whillans ice stream B2. However, we infer that the effective pressure at the channel wall should be of order 200 kPa, which is nearly an order of magnitude greater than the typical values of *Kamb* [2001], and more than an order of magnitude greater than what we infer in this paper and by *Suckale et al.* [2014] at the center of Whillans ice stream B2. Thus h near the channel should be substantially reduced from the 2 to 3 mm values from *Kamb* [2001], although we cannot yet quantify by how much.

5.3. Margin migration and channelized drainage

As mentioned before, we neglected to model the effect of margin migration and lateral advection of cold ice into the shear margin from the ridge. This choice followed the results of *Suckale et al.* [2014] which showed it is impossible to closely match the observed surface velocity profile when lateral advection is accounted for. Ice deformation history within the margin can be complex, with inflow of ice from the ridge occurring alongside inward or outward migration of the shear margin [*Harrison et al.*, 1998; *Echelmeyer and Harrison*, 1999; *Clarke et al.*, 2000]. Furthermore, throughout this paper we have assumed that the thermal structure of the margin has reached a steady state. This means that we assume that net margin migration rate (margin migration minus lateral inflow of cold ice from the ridge into the margin, see *Echelmeyer and Harrison* [1999] for details) is sufficiently low that the ice resides in the shear margin long enough to be warmed to steady state by shear heating. However, one can imagine a scenario in which the margin is migrating, either with a slow steady velocity or perhaps in rapid steps, and a steady state is never reached. We recognize that neglecting lateral advection and assuming a steady state are important caveats in our modeling, which should be a focus for continuing research.

Finally, we have also ignored the possibility that the channel might cut into the till instead of entirely in the ice. We understand that this would change our estimates for $(\sigma_0 - p_{ch})$, though we note that any form of drainage channel operating at a pore pressure much lower than the ice overburden should lead to strengthening of the bed within the margin

6. Conclusion

In this paper we demonstrated that subglacial hydrological processes may select the location of ice stream shear margins. Our mechanism depends upon melt generated in temperate ice at the shear margin, which *Suckale et al.* [2014] showed must be present to explain surface velocity observations, collecting in a drainage channel at the base of the shear margin. As shown by *Röthlisberger* [1972] and *Weertman* [1972], this channel operates at a lower water pressure than the surrounding bed. For the Coulomb-plastic rheology appropriate for subglacial till [*Tulaczyk et al.*, 2000] this decreased water pressure leads to a significant increase in basal strength in the immediate vicinity of the channel. If this basal strengthening exceeds a critical magnitude then we find a smooth transition from a slipping to a locked bed, and thus a stable shear margin configuration selected purely by subglacial hydrological processes. While we develop our arguments for a drainage channel incised into the ice, any efficient subglacial drainage system operating at a depressed pore pressure will provide a similar result.

One fruitful direction for future research may be to investigate how the mechanisms that select the shear margin location vary in the downstream direction. Since the water flux in the channel depends on the distance from the onset of ice streaming, and the hydrological mechanism suggested here becomes more efficient as the flux in the channel increases, we expect subglacial hydrological processes to be most likely to select the shear margin location in the downstream portion of an ice stream.

Appendix A: Model of subglacial channel at the margin

In this appendix we estimate the diameter and the water pressure of a semi-circular R-channel collecting the water generated in the temperate ice region of a margin. Frictional heating within the temperate ice generates melt at a rate per unit of volume $\dot{m}$ set by

$$\dot{m} = \frac{2\tau_E \dot{\epsilon}_E}{L}. \tag{A1}$$

This water will form a system of veins at three-grain junctions allowing the melt to flow through the ice [*Nye*, 1989; *Lliboutry*, 1996]. If the temperate ice is sufficiently impermeable then the melt content of the ice may increase, which will lower the ice viscosity, though we ignore this complication for now. Using the power law rheology from equation (3) the melt rate per unit of volume becomes

$$\dot{m} = (2A_{melt})^{-1/3} |\nabla u|^{4/3} L^{-1}, \tag{A2}$$

where $A_{melt}^{-1/3}$ is 244 kPa.yr$^{1/3}$ for the pressure-dependent melting temperature of -0.6°C [*Cuffey and Paterson*, 2010].

Our model assumes that all of the melt produced in the shear margin is collected in a single drainage channel, operating at a reduced water pressure [*Röthlisberger*, 1972] either by porous flow through temperate ice directly to the channel or first via vertical flow to the bed followed by lateral flow along the ice-till interface. The total volumetric melt rate produced per unit downstream length in the temperate ice can be found by integrating the total shear heating in the temperate zone Ω,

$$\int\int_\Omega (2A_{melt})^{-1/3} |\nabla u|^{4/3} (\rho_w L)^{-1} \mathrm{d}\Omega. \tag{A3}$$

We find values of 37 and 46 m^2 yr^{-1} respectively with and without the subglacial hydrological model in our simulations. These estimations are consistent with previous estimates using a simplified one-dimensional model [*Perol and Rice*, 2011].

We can estimate the ice permeability and porosity in the temperate ice by considering a vertical column of ice in which all water flow is vertical. *Vogel et al.* [2005] drilled to the bottom of Kamb ice stream at the transition between the active upper part and its stopped main trunk, and found that basal ice is devoid of air. We suppose that, at the base of the ice sheet, the veins are water saturated and the ice grains slide at their boundary allowing the water pressure to be equal to the ice overburden stress. This ignores a distribution of suction in the pore water whose distribution is beyond the scope of the present paper. The sliding allows the permeability to adjust to whatever value is needed to transmit the meltwater generated, at least for a system operating in steady state. The total vertical downward flux of meltwater per unit area produced by shear heating above the channel wall may be approximated through Darcy's law,

$$q_w = -\frac{k_{ice}}{\mu_w}\left(\frac{\mathrm{d}p}{\mathrm{d}z} + \rho_w g\right), \tag{A4}$$

where $\mu_w = 1.8 \times 10^{-3}$ N.s.m^{-2} is the dynamic viscosity of water. Thus, the required temperate ice permeability, a function of the downward water flux, is

$$k_{ice} = \frac{q_w\,\mu_w}{(\rho_w - \rho_{ice})\,g}. \tag{A5}$$

A typical value of the flux is approximately 20 mm yr^{-1} [*Perol and Rice*, 2011; *Suckale et al.*, 2014] resulting in an ice permeability of approximately 1.3×10^{-15} m^2. This is consistent with the measurements of water saturated veins from *Jordan and Stark* [2001], which found permeabilities of 1 to 3×10^{-15} m^2 in temperate ice.

According to *Nye and Frank* [1973], for a given k_{ice}, the porosity is proportional to d_g^{-1}, where d_g is the grain size. Our estimation of the permeability at the bed of the ice sheet at the margin is compatible with a porosity of 1.5×10^{-3} for a grain size of 10 mm and 1.5×10^{-4} for a grain size of 1 mm. These values, certainly for $d_g = 1$ mm, and likely for $d_g = 10$ mm, seem small enough that we can assume that the porosity we encounter has a negligible effect on the ice rheology.

A1. Channel diameter

We assume that the water pressure gradient in the channel is negligible – and thus water flow in the channel is driven only by the downslope component of gravity. Using Manning's formula for a turbulent rough-walled channel flow and letting Q_w (m^3 yr^{-1}) be the water flux in the channel, the mean flow velocity is given by

$$\frac{Q_w}{A_c} = \frac{R_h^{2/3}(\sin\alpha)^{1/2}}{n_m}, \tag{A6}$$

where R_h is the hydraulic radius, A_c is the cross-sectional area of the channel, and n_m (in s.m$^{-1/3}$) is the Gaukler-Manning-Strickler roughness coefficient. We further assume that the channel is melted into the ice and has a semi-circular shape. As pointed out by *Clarke* [2003], the Manning roughness coefficient is a wetted-perimeter-average value for this configuration. We can thus distinguish between the roughness of the ice wall, which has wetted perimeter $\pi D/2$, and the bed wall, which has a wetted perimeter D. The hydraulic radius represents the ratio of A_c to wetted perimeter, and can be expressed as

$$R_h = \frac{D}{4(1+2/\pi)}. \tag{A7}$$

Thus, the diameter of this semi-circular channel of constant water pressure that drains a flux Q_w is

$$D = \frac{2^{13/8}\ (Q_w\, n_m)^{3/8}\ (1+2/\pi)^{1/4}}{\pi^{3/8}\,(\sin\alpha)^{3/16}}. \tag{A8}$$

If this tunnel collects a constant supply of 27 m^2 yr^{-1} [*Perol and Rice*, 2011; *Suckale et al.*, 2014] from 100 km upstream the flux in the channel is $Q_w = 0.086$ m^3 s^{-1}. The last parameter that needs to be constrained is the Manning roughness coefficient. Because n_m seems to be often overestimated in subglacial conduits [*Clarke*, 2003], we divert here to a brief discussion about plausible values for our subglacial drainage system.

The value of n_m can be linked to the Nikuradse wall-roughness k, which has units of length, using dimensional analysis. Comparing with experiments of rough-walled turbulent pipe flow at high Reynolds number where the Darcy-Weisbach friction factor is independent of Reynolds number (for example *Gioia and Chakraborty* [2006]) leads to

$$n_m \approx \frac{k^{1/6}}{8g^{1/2}}. \tag{A9}$$

Hence, the Manning roughness coefficient range of 0.02 to 0.04 s.m$^{-1/3}$ inferred by *Clarke* [2003] for subglacial flooding is equivalent to a Nikuradse roughness of 1.6 to 101.1 cm (see Table 2). A wall roughness of 101.1 cm caused by large blocks of ice is rather sensible for a subglacial flooding event; however, in our subglacial drainage case, we assume a plausible range of 0.02 to 0.03 s.m$^{-1/3}$ for n_m corresponding to a Nikuradse roughness of 1.6 to 18.0 cm.

Using this range of values for n_m and our estimate for the water flux in the channel of $Q_w = 0.086$ m^3 s^{-1} we calculate channel diameter of $D = 0.7$ m for $n_m = 0.02$ s.m$^{-1/3}$, and $D = 0.9$ m for $n_m = 0.03$ s.m$^{-1/3}$. Predictions for the channel diameter over a wider range of parameters can be found in Table 2.

A2. Effective pressure in channel

The standard theory for subglacial drainage channels predicts that the water pressure in the channel decreases as the flux in the channel increases [*Röthlisberger*, 1972; *Shreve*, 1972; *Weertman*, 1972; *Nye*, 1976]. Thus, if an R-channel at the shear margin collects a large amount of meltwater we expect a high effective pressure along the ice-till interface immediately adjacent to the channel.

We assume that the channel is incised in temperate ice implying that both the water and the ice temperature are at the melting point. Energy is dissipated within the channel at a rate of $\rho_w g Q_w \sin\alpha$, which leads to melting of the ice wall at a rate u_{melt} controlled by

$$L\rho_{ice}(\pi D/2)\,u_{melt} = \rho_w g Q_w \sin\alpha. \tag{A10}$$

The expansion of the channel due to melting is balanced by creep closure of the channel due to the difference between the water pressure in the channel and the ice overburden. We estimate the creep closure rate using the solution from *Nye* [1953],

$$u_{creep} = \frac{D/2}{27} A_{melt}\,(\sigma_0 - p_{ch})^3\,. \tag{A11}$$

For a steady state channel the creep closure exactly balances melting at the ice wall (i.e. $u_{creep} = u_{melt}$) leading to,

$$(\sigma_0 - p_{ch})^3 = 27\,\frac{\rho_w g \sin\alpha Q_w}{\pi L\,\rho_{ice}\,A_{melt}\,(D/2)^2}. \tag{A12}$$

Recalling that Q_w and the channel diameter are related by equation (A8), we find that the effective pressure inside the R-channel is

$$(\sigma_0 - p_{ch}) = K_2\,\frac{Q_w^{1/12}\,(\sin\alpha)^{11/24}}{n_m^{1/4}\,A_{melt}^{1/3}}, \tag{A13}$$

where

$$K_2 = \left(\frac{\rho_w g}{\rho_{ice} L_f K_1}\right)^{1/3} \tag{A14}$$

and $K_1 = (2/27)\,(2\pi)^{1/4}\,(1+2/\pi)^{1/2}$.

A water flux $Q_w = 0.086$ m^3 s^{-1} is consistent with an effective pressure $(\sigma_0 - p_{ch})$ in the R-channel ranging from 389 to 550 kPa for reasonable values of the Manning coefficient (see Table 2). From the simulation of *Suckale et al.* [2014] displayed in Figure 6A1 the inferred width-averaged basal drag at the Whillans B2 ice stream center is 3.7 kPa. Therefore, using $f = 0.5$ [*Rathbun et al.*, 2008] and $c = 1$ kPa [*Kamb*, 2001], the yield strength of the bed $\tau_{yield} = f(\sigma_0 - p) + c$ near a channel of diameter $D = 0.9$ m is 78 times larger than the predicted yield strength at the center of the Whillans ice stream B2.

A3. Sensitivity analysis and limitations of the channelized drainage model

Table 2. Semi-circular R-channel diameter D, and effective pressure for different discharge rates Q_w and Manning coefficients n_m (with corresponding Nikuradse roughness amplitudes k shown).

Parameter	notation [units]	values			
Manning coefficient	n_m [$\mathrm{s\,m^{-1/3}}$]	0.01	0.02	0.03	0.04
Equivalent Nikuradse roughness	k [cm]	0.03	1.6	18.0	101.1
	Water discharge of $Q_w = 0.086\ \mathrm{m^3\,s^{-1}}$				
Channel diameter	D [m]	0.6	0.7	0.9	1.0
Effective pressure	$(\sigma_0 - p_{ch})$ [kPa]	550	462	419	389
	Water discharge of $Q_w = 0.022\ \mathrm{m^3\,s^{-1}}$				
Channel diameter	D [m]	0.3	0.4	0.5	0.6
Effective pressure	$(\sigma_0 - p_{ch})$ [kPa]	490	413	374	347

As shown by *Suckale et al.* [2014], the size of the temperate region and, hence, the meltwater generated at the bed varies significantly with factors such as margin migration or surface crevassing. Also, some melt may migrate towards the center of the ice stream due to the transverse slope of the bed and ice surface near the margin [*Le Brocq et al.*, 2009; *Fricker and Scambos*, 2009] – leading to a lower flux in the channel than that predicted by relation (A3). Furthermore, we estimated the water flux for a channel that has captured meltwater along 100 kilometers in the downstream direction. Near the region where the ice stream initiates such water flow is greatly reduced. Considering the uncertainties, relation (A3) may overestimate the water flux in the channel. Nevertheless, we find that reducing the estimated value of Q_w by a factor 4 in equations (A8) and (A13) results in only an 11% reduction of $(\sigma_0 - p_{ch})$ and a 44% reduction in D (Table 2). Therefore, our estimates of bed strength next to the channel and D are not strongly sensitive to the assumed magnitude of the water flux in the channel Q_w.

It is also important to note the channel creep closure model adopted here neglects any anti-plane strain rate components, which are thought to be large at the locking point. *Weertman* [1972] and *Röthlisberger* [1972] noted that the coupling between in-plane and anti-plane strain rates in a nonlinear material may lead to a higher creeping rate of the channel wall and, therefore, a lower effective pressure in the channel. Keeping these uncertainties in mind we set the effective pressure in the channel at 200 kPa in our simulations, and we hope to better quantify these effects in future work.

Acknowledgments. This research was supported by the National Science Foundation through the Office of Polar Programs award number 1341499 (March 2014 to February 2017), and previously grant ANT-0739444 (June 2008 to May 2012). The authors thank Timonthy Creyts, Ian Hewitt, Ian Joughin, and Christian Schoof for fruitful discussions. Input files used for the numerical simulations are available upon request by emailing the corresponding author at tperol@seas.harvard.edu. The data used in the paper are from *Echelmeyer et al.* [1994].

References

Bamber, J. L., D. G. Vaughan, and I. Joughin, Widespread Complex Flow in the Interior of the Antarctic Ice Sheet, *Science*, *287*(5456), 1248–1250, doi:10.1126/science.287.5456.1248, 2000.

Barenblatt, G. I., The formation of equilibrium cracks during brittle fracture. General ideas and hypotheses. Axially-symmetric cracks, *J. Appl. Math. Mech.*, *23*(3), 622 – 636, doi:10.1016/0021-8928(59)90157-1, 1959.

Bilby, B. A., A. H. Cottrell, and K. H. Swinden, The spread of plastic yield from a notch, *Proc. R. Soc. Lond. A.*, *272*(1350), 304–314, doi:10.1098/rspa.1963.0055, 1963.

Bindschadler, R., and P. Vornberger, Changes in the west antarctic ice sheet since 1963 from declassified satellite photography, *Science*, *279*(5351), 689–692, doi: 10.1126/science.279.5351.689, 1998.

Clarke, G. K. C., Hydraulics of subglacial outburst floods: new insights from the spring-hutter formulation, *J. Glaciol.*, *49*(165), 299–313, 2003.

Clarke, T. S., C. Liu, N. E. Lord, and C. R. Bentley, Evidence for a recently abandoned shear margin adjacent to ice stream B2, Antarctica, from ice-penetrating radar measurements, *J. Geophys. Res.*, *105*(B6), 2000.

Creyts, T. T., and C. G. Schoof, Drainage through subglacial water sheets, *J. Geophys. Res.*, *114*(F04008), doi: 10.1029/2008JF001215, 2009.

Cuffey, K., and W. Paterson, *The Physics of Glaciers (Fourth Edition)*, ISBN 9780123694614, Elsevier, 2010.

Dugdale, D., Yielding of steel sheets containing slits, *J. Mech. Phys. Solids*, *8*(2), 100–104, 1960.

Durham, W. B., S. H. Kirby, and L. A. Stern, Creep of water ices at planetary conditions: A compilation, *Journal of Geophysical Research: Planets (1991–2012)*, *102*(E7), 16,293–16,302, 1997.

Echelmeyer, K., and W. Harrison, Ongoing margin migration of Ice Stream B, Antarctica, *J. Glaciol.*, *45*(150), 361–369, 1999.

Echelmeyer, K., W. Harrison, C. Larsen, and J. Mitchell, The role of the margins in the dynamics of an active ice stream, *J. Glaciol.*, *40*(136), 527–538, 1994.

Engelhardt, H., Ice temperature and high geothermal flux at siple dome, west antarctica, from borehole measurements, *J. Glaciol.*, *50*(169), 251–256, doi:10.3189/172756504781830105, 2004.

Engelhardt, H., and B. Kamb, Basal hydraulic system of a West Antarctic ice stream: Constraints from borehole observations, *Journal of Glaciology*, *43*(144), 207–230, 1997.

Fricker, H. A., and T. Scambos, Connected subglacial lake activity on lower Mercer and Whillans Ice Streams, West Antarctica, 20032008, *J. Glaciol.*, *55*(190), 303–315, 2009.

Frost, H. J., and M. F. Ashby, *Deformation mechanism maps: the plasticity and creep of metals and ceramics*, Pergamon press, 1982.

Gioia, G., and P. Chakraborty, Turbulent Friction in Rough Pipes and the Energy Spectrum of the Phenomenological Theory, *Physical Review Letters*, *96*(044502), 2006.

Giovinetto, M., and H. Zwally, Spatial distribution of net surface accumulation on the antarctic ice sheet, *Ann. Glaciol.*, *31*, 2000.

Harrison, W., K. A. Echelmeyer, and C. Larsen, Measurement of temperature in a margin of Ice Stream B, Antarctica : implications for margin migration and lateral drag, *J. Glaciol.*, *44*(148), 1998.

Hewitt, I. J., Modelling distributed and channelized subglacial drainage: the spacing of channels, *J. Glaciol.*, *57*(202), 302–314, doi:10.3189/002214311796405951, 2011.

Hooke, R. L., *Principles of Glacier Mechanics*, Second ed., Cambridge University Press, 2005.

Jacobson, H., and C. Raymond, Thermal effects on the location of ice stream margins, *J. Geophys. Res.*, *103*(B6), 111–122, 1998.

Jordan, R., and J. Stark, Capillary Tension in Rotting Ice Laters, *Tech. rep.*, Technical Report ERDC/CRREL TR-01-13. US Army Corps of Engineers, Cold Regions Research and Engineering Laboratory, 2001.

Joughin, I., S. Tulaczyk, R. Bindschadler, and S. F. Price, Changes in West Antarctic Ice Stream velocities: Observation and analysis, *J. Geophys. Res.*, *107*(B11), doi: 10.1029/2001JB001029, 2002.

Joughin, I., D. R. MacAyeal, and S. Tulaczyk, Basal shear stress of the Ross ice streams from control method inversions, *J. Geophys. Res.*, *109*(B9), doi:10.1029/2003JB002960, 2004.

Kamb, B., Basal zone of the West Antarctic Ice Streams and its role in lubrication of their rapid motion, in *The West Antarctic Ice Sheet: Behavior and Environment*, vol. 77, edited by R. B. Alley and R. A. Bindschadler, pp. 157–199, AGU, Washington, DC, doi:10.1029/AR077p0157, 2001.

Kyrke-Smith, T., R. Katz, and A. Fowler, Subglacial hydrology and the formation of ice streams, *Proc. Roy. Soc. A*, *470*(2161), doi:10.1098/rspa.2013.0494, 2014.

Le Brocq, A., A. Payne, M. Siegert, and R. Alley, A subglacial water-flow model for West Antarctica, *J. Glaciol.*, *55*(193), 879–888, doi:10.3189/002214309790152564, 2009.

Lliboutry, L., Temperate ice permeability, stability of water veins and percolation of internal meltwater, *J. Glaciol.*, *42*(141), 201–211, 1996.

Maule, C. F., M. E. Purucker, N. Olsen, and K. Mosegaard, Heat flux anomalies in antarctica revealed by satellite magnetic data, *Science*, *309*(5733), 464–467, doi: 10.1126/science.1106888, 2005.

Ng, F. S., Coupled ice-till deformation near subglacial channels and cavities, *Journal of Glaciology*, *46*(155), 580–598, doi: doi:10.3189/172756500781832756, 2000.

Nye, B. F., and F. C. Frank, Hydrology of the intergranular veins in a temperate glacier, *J. Glaciol.*, 1973.

Nye, J., The flow law of ice from measurements in glacier tunnels, laboratory experi- ments and the jungfraufirn borehole experiment, *Proc. R. Soc. Lond. Ser. A 219*, pp. 477–489, 1953.

Nye, J., Water flow in glaciers: jökulhlaups, tunnels and veins, *J. Glaciol.*, *17*(76), 181–207, 1976.

Nye, J., The geometry of water veins and nodes in polycrystalline ice, *J. Glaciol.*, *35*, 17–22, 1989.

Perol, T., and J. R. Rice, Control of the width of West Antarctic ice streams by internal melting in the ice sheet near the margins, abstract C11B-0677 presented at 2011 Fall Meeting, AGU, San Francisco, Calif., 5-9 Dec., 2011.

Perol, T., and J. R. Rice, Shear heating and weakening of the margins of West Antarctic ice streams, *Geophys. Res. Lett.*, doi:10.1002/2015GL063638, 2015.

Rathbun, A., C.Marone, R. Alley, and S. Anandakrishnan, Laboratory study of the frictional rheology of sheared till, *J. Geophys. Res.*, *113*(F02020), doi:10.1029/2007JF000815, 2008.

Rempel, A. W., A theory for ice-till interactions and sediment entrainment beneath glaciers, *Journal of Geophysical Research: Earth Surface*, *113*(F1), doi:10.1029/2007JF000870, 2008.

Rempel, A. W., Effective stress profiles and seepage flows beneath glaciers and ice sheets, *Journal of Glaciology*, *55*(191), 431–443, doi:doi:10.3189/002214309788816713, 2009.

Rice, J., A path independent integral and the approximate analysis of strain concentration by notches and cracks, *Journal of Applied Mechanics*, *35*, 379–386, 1968a.

Rice, J., Mathematical analysis in the mechanics of fracture, in *Fracture: An Advanced Treatise: Vol. 2, Mathematical Fundamentals*, edited by H. Liebowitz, pp. 191–311, Academic Press, N.Y., 1968b.

Rose, K., Characteristics of ice flow in Marie Byrd Land, Antarctica, *Journal of Glaciology*, *24*, 63–75, 1979.

Röthlisberger, H., Water pressure in intra- and subglacial channels, *J. Glaciol.*, *11*(62), 177–203, 1972.

Schoof, C., On the mechanics of ice-stream shear margins, *J. Glaciol.*, *50*(169), 208–218, doi:10.3189/172756504781830024, 2004.

Schoof, C., Thermally-driven migration of ice stream shear margins, *J. Fluid Mech.*, *712*, 2012.

Shabtaie, S., and C. Bentley, West Antarctic Ice Streams Draining into the Ross Ice Shelf: Configuration and Mass Balance, *J. Geophys. Res.*, *92*, 1311–1336, 1987.

Shreve, R., Movement of water in glaciers, *J. Glaciol*, *11*(62), 205–214, 1972.

Smith, B., N. Lord, and C. Bentley, Crevasse ages on the northern margin of Ice Stream C, West Antarctica, *Ann. Glaciol.*, *34*(1), 209–216, doi:10.3189/172756402781817932, 2002.

Spikes, V. B., G. S. Hamilton, S. A. Arcone, S. Kaspari, and P. A. Mayewski, Variability in accumulation rates from GPR profiling on the West Antarctic plateau, *Ann. Glaciol.*, *39*, 2004.

Suckale, J., J. D. Platt, T. Perol, and J. R. Rice, Deformation-induced melting in the margins of the West Antarctic ice streams, *J. Geophys. Res. Earth Surf.*, *119*, doi: 10.1002/2013JF003008, 2014.

Tulaczyk, S., W. B. Kamb, and H. Engelhardt, Basal mechanics of Ice Stream B, West Antarctica 1. till mechanics, *J. Geophys. Res.*, *105*(B1), 463–481, doi:10.1029/1999JB900329, 2000.

Vogel, S. W., S. Tulaczyk, B. Kamb, H. Engelhardt, F. D. Carsey, A. E. Behar, A. L. Lane, and I. Joughin, Subglacial conditions during and after stoppage of an Antarctic Ice Stream: Is reactivation imminent?, *Geophys. Res. Lett.*, *32*, doi:10.1029/2005GL022563, 2005.

Weertman, J., General theory of water flow at base of a glacier or ice sheet, in *Reviews of Geophysics and Space physics*, vol. 10, pp. 287—333, American Geophysical Union, doi: 10.1029/RG010i001p00287, 1972.

Whillans, I., and C. Van Der Veen, New and improved determinations of velocity of Ice Streams B and C, West Antarctica, *J. Glaciol.*, 1993.

Whillans, I., and C. Van der Veen, The role of lateral drag in the dynamics of Ice Stream B, Antarctica, *J. Glaciol.*, *43*(144), 231–237, 1997.

Zotikov, I., *The Thermophysics Of Glaciers*, D. Reidel, Mass, 1986.

Corresponding author: Thibaut Perol, School of Engineering and Applied Sciences, Harvard University, Pierce Hall 327, 29 Oxford Street, Cambridge, MA 02138, USA (tperol@seas.harvard.edu)